Chinese Journal of Natural Medicines

Hernandezine promotes cancer cell apoptosis and disrupts the lysosomal acidic environment and cathepsin D maturation

Qianwen FENG, Lu SUN, Jibran Sualeh Muhammad, Qingli ZHAO, Songji ZHAO, Zhengguo CUI, Hidekuni INADERA

Citation: Qianwen FENG, Lu SUN, Jibran Sualeh Muhammad, Qingli ZHAO, Songji ZHAO, Zhengguo CUI, Hidekuni INADERA, Hernandezine promotes cancer cell apoptosis and disrupts the lysosomal acidic environment and cathepsin D maturation, Chinese Journal of Natural Medicines, 2024, 22(5), 387−401. doi: 10.1016/S1875−5364(24)60638−2.

View online: https://doi.org/10.1016/S1875−5364(24)60638−2

Available online at www.sciencedirect.com
ScienceDirect
Chinese Journal of Natural Medicines 2024, **22**(5): 387-401
doi: 10.1016/S1875-5364(24)60638-2
Chinese Journal of Natural Medicines

•Original article•

Hernandezine promotes cancer cell apoptosis and disrupts the lysosomal acidic environment and cathepsin D maturation

FENG Qianwen[1], SUN Lu[2], Muhammad Jibran Sualeh[3], ZHAO Qingli[4], ZHAO Songji[5], CUI Zhengguo[6*], INADERA Hidekuni[1*]

[1] *Department of Public Health, Graduate School of Medicine and Pharmaceutical Sciences, University of Toyama, Toyama 930-8501, Japan;*
[2] *Department of Pediatric Cardiology, Heart Center, Guangzhou Women and Children's Medical Center, Guangzhou Medical University, Guangzhou 510000, China;*
[3] *Department of Basic Medical Sciences, College of Medicine, University of Sharjah, Sharjah 57545, United Arab Emirates;*
[4] *Department of Radiology, Graduate School of Medicine and Pharmaceutical Sciences, University of Toyama, Toyama 930-8501, Japan;*
[5] *Advanced Clinical Research Center, Fukushima Global Medical Science Center, Fukushima Medical University, Fukushima City, Fukushima 960-8074, Japan;*
[6] *Department of Environmental Health, School of Medical Sciences, University of Fukui, Fukui 910-8580, Japan*

Available online 20 May, 2024

[ABSTRACT] Hernandezine (Her), a bisbenzylisoquinoline alkaloid extracted from *Thalictrum flavum*, is recognized for its range of biological activities inherent to this herbal medicine. Despite its notable properties,the anti-cancer effects of Her have remained largely unexplored. In this study, we elucidated that Her significantly induced cytotoxicity in cancer cells through the activation of apoptosis and necroptosis mechanisms. Furthermore, Her triggered autophagosome formation by activating the AMPK and ATG5 conjugation systems, leading to LC3 lipidation. Our findings revealed that Her caused damage to the mitochondrial membrane, with the damaged mitochondria undergoing mitophagy, as evidenced by the elevated expression of mitophagy markers. Conversely, Her disrupted autophagic flux, demonstrated by the upregulation of p62 and accumulation of autolysosomes, as observed in the RFP-GFP-LC3 reporter assay. Initially, we determined that Her did not prevent the fusion of autophagosomes and lysosomes. However, it inhibited the maturation of cathepsin D and increased lysosomal pH, indicating an impairment of lysosomal function. The use of the early-stage autophagy inhibitor, 3-methyladenine (3-MA), did not suppress LC3II, suggesting that Her also induces noncanonical autophagy in autophagosome formation. The application of Bafilomycin A1, an inhibitor of noncanonical autophagy, diminished the recruitment of ATG16L1 and the accumulation of LC3II by Her, thereby augmenting Her-induced cell death. These observations imply that while autophagy initially plays a protective role, the disruption of the autophagic process by Her promotes programmed cell death. This study provides the first evidence of Her's dual role in inducing apoptosis and necroptosis while also initiating and subsequently impairing autophagy to promote apoptotic cell death. These insights contribute to a deeper understanding of the mechanisms underlying programmed cell death, offering potential avenues for enhancing cancer prevention and therapeutic strategies.

[KEY WORDS] Hernandezine; Apoptosis; Mitophagy; Autophagic flux; Lysosome; Noncanonical autophagy
[CLC Number] R965 **[Document code]** A **[Article ID]** 2095-6975(2024)05-0387-15

Introduction

Cancer remains a critical global health challenge, consistently ranking as one of the leading causes of mortality, with nearly ten million deaths reported worldwide in 2020. Breast cancer, lung cancer, and stomach cancer emerge as the most commonly diagnosed forms of this disease [1]. Deepening our comprehension of the mechanisms that govern cancer cell death is pivotal for developing strategies to counteract chemoresistance [2]. Within the current research paradigm, a principal objective is to identify compounds capable of selectively enhancing cancer cell susceptibility to cell death. In this regard, numerous natural products have been identified as potent inducers of programmed cell death across various cancer types [3, 4].

Mitophagy, or mitochondrial macroautophagy, repres-

[Received on] 23-Nov.-2023
[Research funding] This work was supported by JSPS KAKENHI (Nos. 20K10449 and 23K09645).
[*Corresponding author] E-mails: sai@u-fukui.ac.jp (CUI Zhengguo); inadera@med.u-toyama.ac.jp (Inadera Hidekuni)
These authors have no conflict of interest to declare.

ents a specialized variant of autophagy dedicated to the selective degradation of damaged, dysfunctional, or senescent mitochondria through the autophagic machinery [5–8]. This process is governed by various intracellular mechanisms that ensure the targeted delivery of compromised mitochondria to autophagosomes for degradation. Consequently, a natural compound that can simultaneously enhance mitophagy and autophagosome formation yet inhibit the degradation process within autolysosomes holds significant promise as a chemotherapeutic agent [9]. Such a strategy leverages the cell's intrinsic degradation pathways to eliminate cancer cells effectively, providing a novel avenue for cancer therapy development.

Hernandezine (Her, Fig. 1A) is a bisbenzylisoquinoline alkaloid isolated from the Chinese medicinal herb *Thalictrum flavum*. Studies have documented its anticancer properties across a variety of cancers, including hepatocellular carcinoma, cervical cancer, pancreatic cancer, and melanoma [10–13]. As an activator of AMP-activated protein kinase (AMPK), Her induces autophagy-mediated and caspase-independent cell death, exhibiting low toxicity [13]. Similarly, neferine, tetrandrine, berbamine, and other structurally related compounds have shown anti-tumor efficacy across diverse cancer types by engaging both apoptosis and autophagy pathways [14–16]. Despite these findings, the specific role of autophagy in Her's anticancer effects remains to be fully understood, necessitating further exploration. Of particular interest is the impact of autophagic flux on breast cancer, gastric cancer, and lung cancer cell lines, which has not yet been investigated.

This study aimed to elucidate the molecular pathways through which Her influences cancer cell death, with a specific focus on its regulatory effects on the autophagy-mediated apoptosis process. Our objectives included determining the impact of Her on autophagy inhibition and its subsequent influence on the apoptotic cell death pathway. Furthermore, we sought to analyze how Her modulates the expression of specific targets involved in controlling autophagy blockage-mediated apoptotic cell death. By achieving a comprehensive understanding of the molecular mechanisms underlying various forms of cell death, this study aims to underscore the potential applicability of Her in cancer therapy.

Materials and Methods

Chemicals, inhibitors, and antibodies

Her was purchased from LATOXAN (Portes-lès-Valence, France Table 1). Necrostatin-1 (Nec-1; a RIP1 inhibitor) and necrosulfonamide (NSA; a mixed-lineage kinase domain-like protein (MLKL) inhibitor) were purchased from Cayman Chemical (Ann Arbor, MI). 3-Methyladenine (3-MA; a PI3K inhibitor) and hydroxychloroquine (HCQ; an autophagy inhibitor) were obtained from Tokyo Chemical Industry Co., Ltd. (Tokyo, Japan). Z-VAD-FMK (pan-caspase inhibitor) was purchased from Selleck Chemicals (Shanghai, China). All compounds were solubilized as recommended. Bafilomycin A1 (Baf A1, a V-ATPase inhibitor) and Rapa (an autophagy activator or mTORC1 complex inhibitor) were purchased from Cell Signaling Technologies, Inc. (Danvers, MA). Prestained Protein Size Marker Ⅲ and dimethyl sulfoxide (DMSO) were obtained from Wako Pure Chemical Industries Ltd. (Osaka, Japan). LysoTracker™ Red DND-99, LysoSensor DND-160, and MitoTracker™ Red CMXRos were purchased from Invitrogen (Waltham, MA). Acridine orange (AO) stain was obtained from Sigma-Aldrich (St. Louis, MO).

Cell culture and treatment

Human gastric cancer (AGS; RRID: CVCL_0139), human breast epithelial (MCF-7; RRID: CVCL_0031), and human lung adenocarcinoma (A549; RRID: CVCL_0023) cell lines were obtained from the Japan Cancer Research Resources Bank (Tokyo, Japan). Cells were grown in RPMI-1640 containing 10% heat-inactivated fetal bovine serum (FBS) and maintained in a humidified incubator (5% CO_2, 37 °C). Cell lines were seeded overnight and treated with Her with or without inhibitors at various concentrations and time points, as indicated in the Results.

Cell viability assay

The 3-[4,5-dimethylthiazol-2-yl]-2,5 diphenyl tetrazolium bromide (MTT) assay was utilized to assess cell viability. Initially, cells were plated at a density of 1×10^4 cells/well in 96-well plates and cultured overnight. Subsequently, MTT solution was added to each well at a concentration of 0.05 $mg \cdot mL^{-1}$, followed by incubation for 4 h at 37 °C. After incubation, dimethyl sulfoxide (DMSO) was added to dissolve the formazan crystals formed. To ensure accuracy, each concentration was tested in three parallel wells. The absorbance was measured at 490 nm using a microplate reader (Multiskan FC Microplate Photometer, Thermo Scientific, Waltham, MA), providing a quantitative measure of cell viability across various conditions.

Colony formation assay

Cells, seeded in 6-well plates, were treated with Her for 24 h. Following this treatment, the culture medium was replaced, and the culture was continued for an additional two weeks. After this period, the medium was removed, and the cells were washed twice with phosphate-buffered saline (PBS). The cells were then fixed with 4% paraformaldehyde for 30 min and stained with crystal violet for 1 h at room temperature. Subsequently, the plates were thoroughly rinsed with water and left to air dry at room temperature. This procedure facilitated the visualization of cell colonies, providing insights into the effects of Her on cell proliferation and survival over an extended culture period.

Apoptosis assessment

The assessment of cell apoptosis was conducted using the Dead Cell Apoptosis Kit with Annexin V FITC and PI, designed for flow cytometry (Invitrogen), in combination with the FACS Canto II system (BD Biosciences, Franklin Lakes, NJ), adhering strictly to the manufacturers' guidelines. The collected data were then analyzed using FlowJo software.

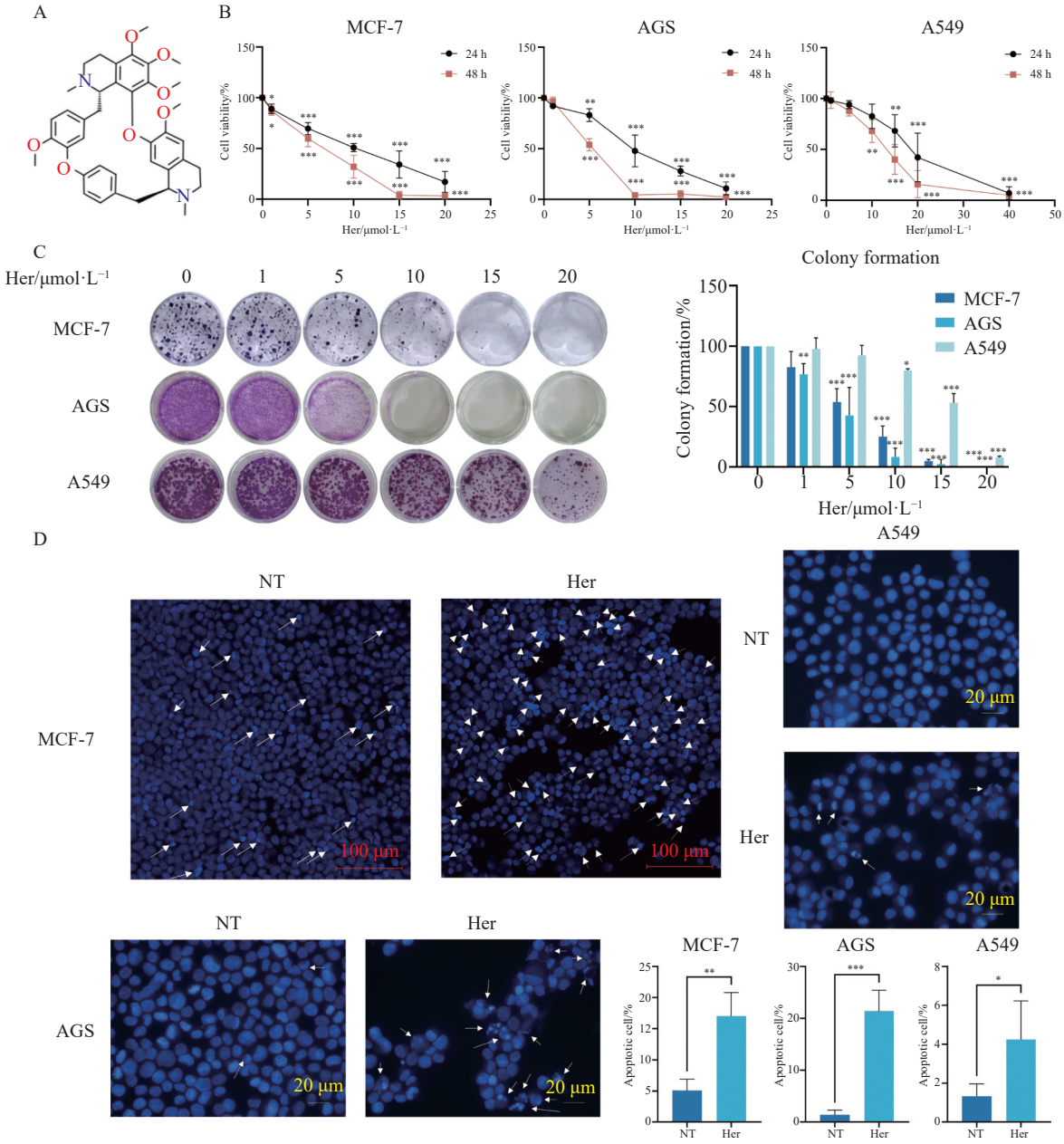

Fig. 1 Effects of Her on the viability and growth of cancer cells. (A) Chemical structure of Her. (B) Cell viability was measured by MTT assays after Her treatment for 24 h and 48 h using MCF-7, AGS, and A549 cells. (C) Colony formation after treatment with Her for 24 h and culture for two weeks. Statistical analysis of colony formation. (D) Morphological changes were detected by Hoechst staining. MCF-7 (200 ×), AGS, and A549 (400 ×) cells were cultured with or without Her for 24 h. The white arrows indicated nuclear condensation and nuclear fragmentation. A semi-quantitative analysis was performed for Fig. 1D. Data are presented as means ± SD (*n* = 3). $^{*}P < 0.05$, $^{**}P < 0.01$, $^{***}P < 0.001$ *vs* control.

Sub-G1 DNA content analysis

Sub-G1 DNA content analysis was performed as previously described [17]. Cells subjected to treatment were harvested and resuspended in PBS. To fix the cells, 70% (*V*/*V*) cold ethanol was added, and the cells were stored at −20 °C for no more than two weeks until further analysis. Following storage, cells were centrifuged, and the supernatant was discarded. The cells then underwent two PBS washes. Subsequently, cells were resuspended in PBS containing DNA extraction buffer and incubated for 5 min at room temperature. After another centrifugation step and removal of the supernatant, the cells were resuspended in DNA staining solution, comprising 200 μg·mL^{-1} DNase-free RNase and 20 μg·mL^{-1} propidium iodide (PI), and incubated at room temperature for a minimum of 30 min before flow cytometry analysis. Data obtained from flow cytometry were analyzed using ModFit software.

Morphological observation

Following treatment, cells were collected, rinsed with PBS, and fixed using 4% paraformaldehyde in PBS for 30 min at

Table 1 Source and product number of antibodies

Antibody	Company	Catalog
Anti-β-actin antibody	Wako Pure Chemical Industries (Osaka, Japan)	013-24553
Bcl-2	Santa Cruz Biotechnology	sc-7382
JNK	Santa Cruz Biotechnology	sc-7345
p-JNK	Santa Cruz Biotechnology	sc-6254
Bax	Santa Cruz Biotechnology	sc-20067
AMPK Pathway Explorer Antibody MiniPack (p-AMPK Thr172, AMPK)	Millipore (Burlington, MA)	15-115
AlexaFluor488 conjugated anti-rabbit secondary antibody	Invitrogen (Waltham, MA)	A11008
AlexaFluor488 conjugated anti-mouse secondary antibody	Invitrogen	A11001
AlexaFluor647-conjugated anti-rabbit secondary antibody	Invitrogen	A32733
LC3B	Cell Signaling Technology (Danvers, MA)	83506
LC3A/B	Cell Signaling Technology	12741
p62	Cell Signaling Technology	8025
c-PARP	Cell Signaling Technology	5625
XIAP	Cell Signaling Technology	2045
p-ERK1/2 (p-p44/42)	Cell Signaling Technology	4370
ERK1/2 (p44/42)	Cell Signaling Technology	4695
c-caspase 3	Cell Signaling Technology	9661
c-caspase7	Cell Signaling Technology	8438
ATG5	Cell Signaling Technology	2630
ATG16L	Cell Signaling Technology	8089
p-p38	Cell Signaling Technology	4511
p38	Cell Signaling Technology	8690
the Mitophagy Antibody Sampler Kit	Cell Signaling Technology	43110
anti-rabbit secondary antibodies	Cell Signaling Technology	7074
anti-mouse secondary antibodies	Cell Signaling Technology	7076
Mcl-1	BD Biosciences (Franklin Lakes, NJ)	559027
NOXA	Abcam (Cambridge, UK)	ab13654

4 °C. Subsequently, they were stained with 1 mmol·L^{-1} Hoechst 33258 for 5 min to facilitate DNA visualization. Observations were conducted under a confocal microscope (LSM780, Carl Zeiss, Jena, Germany) or a fluorescence microscope (BX-61, Olympus, Tokyo, Japan), utilizing a 400 × objective lens. The total cell count and the number of cells that had undergone apoptosis were tallied. The apoptosis rate was then calculated based on the analysis of three or more images captured in completely distinct areas.

Western blotting assay

After treatment, cells were thoroughly washed with PBS three times, followed by lysis using RIPA buffer that included protease and phosphatase inhibitors to extract proteins. The lysates were then centrifuged at 13,000 r·min^{-1} for 10 min at 4 °C, and the supernatants were collected into separate tubes. Protein concentrations were quantified using the Bradford Protein Assay Kit, with absorbance readings taken at 560 nm on a microplate reader. An equal amount of protein from each sample was subjected to electrophoresis, followed by transfer onto PVDF membranes (Millipore). These membranes were blocked for 2 h in 1× Tris-buffered saline with 0.1% Tween 20 (TBST) containing 5% non-fat milk. Subsequently, they were incubated overnight at 4 °C with the appropriate primary antibody. After washing with TBST, HRP-labelled secondary antibody was applied for 2 h at room temperature. Target proteins were visualized using the Immobilon Classico Western HRP Substrate (Millipore).

Confocal microscopy

For live-cell imaging, cancer cells were plated on a 35 mm glass-bottom dish (MATSUNAMI GLASS IND., LTD., Osaka, Japan) to allow for attachment overnight. To visualize lysosomes and mitochondria, cells were incubated with 100 nmol·L^{-1} LysoTracker Red or 100 nmol·L^{-1} MitoTracker Red, respectively, for 1 h at 37 °C. Following this incubation, cells were fixed with 4% paraformaldehyde for 10 min at room temperature and subsequently washed three times for 5 min with 1× PBS containing 0.1% Tween 20 (PBST). Permeabilization was achieved with PBS containing 0.1% Tri-

ton X-100 for 10 min, followed by three PBS washes. To prevent non-specific antibody binding, cells were incubated in 5% BSA in PBST for 1 h. Overnight incubation at 4 °C with the primary antibody diluted in 1% BSA in PBST was then performed, followed by washing and incubation with the secondary antibody for 1 h in the dark at room temperature. For multicolor staining, the process was repeated with a second set of primary and secondary antibodies.

Autophagic flux was monitored using the Premo™ Autophagy Tandem Sensor RFP-GFP-LC3B Kit according to the manufacturer's instructions. Following cell seeding, 2 μL of the Premo™ Autophagy Sensor was added per 1×10^4 cells in the medium and incubated at 37 °C for 16 h. Treatment with 20 μmol·L^{-1} Her, 30 μmol·L^{-1} CQ, and Rapa as a positive control was then administered. GFP and RFP signals were imaged, and the number of puncta per cell was quantified using ImageJ from at least three different areas.

For pH detection, cells were loaded with 5 μmol·L^{-1} LysoSensor or 1 μg·mL^{-1} acridine orange (AO) staining solution for 5 min prior to detection.

Subcellular fluorescence was observed using a Carl Zeiss LSM780 laser scanning confocal microscope. The intensity of colocalization and Pearson correlation coefficients (*R* values) for fluorophore colocalization were calculated using the Colocalization Threshold and Coloc 2 functions in ImageJ.

Cellular ROS assay

Changes in reactive oxygen species (ROS) levels were assessed using DCFH-DA staining (Molecular Probes, Eugene, OR). In brief, cells were incubated with 20 μmol·L^{-1} DCFH-DA for 15 min at 37 °C. Following the incubation, cells were washed twice with PBS to remove any excess dye. The ROS levels within the cell population were then quantified by flow cytometry, adhering to the manufacturer's guidelines.

Mitochondrial membrane potential (MMP)

The cationic fluorophore tetramethylrhodamine methyl ester perchlorate (TMRM), utilized for staining mitochondria and their matrix, offers insights into mitochondrial health. Following treatment for the specified duration, cells were harvested and exposed to 1 μmol·L^{-1} TMRM (Molecular Probes) dissolved in PBS supplemented with 1% FBS for 15 min at 37 °C. The decrease in MMP, indicative of mitochondrial dysfunction, was then quantitatively assessed using flow cytometry in accordance with the manufacturer's instructions.

Statistical analysis

All experiments were conducted with three independent biological replicates. Results were expressed as means ± standard deviation (SD). For statistical analysis, we employed GraphPad Prism 7 (GraphPad Software, La Jolla, CA). The software ImageJ was utilized for quantifying relative protein expression from Western blot images, calculating Pearson's correlation coefficients, and assessing puncta per cell from confocal microscopy images. We have presented representative images from one of the three independent replicates for illustration. Comparative analysis of groups was conducted using either one-way ANOVA or Student's *t*-test. *P*-value less than 0.05 was deemed to indicate statistical significance, guiding the interpretation of our results.

Results

Effects of Her on cell viability in multiple types of cancer cells

We assessed the impact of Her on the proliferation and survival of three cancer cell lines: MCF-7 (breast cancer), AGS (gastric cancer), and A549 (lung cancer). Each cell line exhibited a marked reduction in cell viability that was both time- and dose-dependent upon increasing concentrations of Her (Fig. 1B). Specifically, in MCF-7 cells, viability decreased by 50% following 24-hour treatment with 8.94 μmol·L^{-1} Her or after 48 h with 5.88 μmol·L^{-1} Her. For AGS cells, a 50% reduction in viability occurred after 24 h with 9.63 μmol·L^{-1} Her and after 48 h with 5.18 μmol·L^{-1} Her. However, A549 cells demonstrated similar viability reductions at considerably higher concentrations of Her, with a 50% decrease observed following 24-hour treatment with 18.29 μmol·L^{-1} Her and after 48 h with 12.46 μmol·L^{-1} Her. Furthermore, a colony formation assay conducted over a two-week period revealed nearly complete inhibition of growth in MCF-7 cells treated with 15 μmol·L^{-1} Her and in AGS cells treated with 10 μmol·L^{-1} Her (Fig. 1C). These findings indicate that Her treatment effectively inhibits cell proliferation and induces cytotoxic effects across all examined cancer cell lines.

Effects of Her on apoptosis and apoptosis-related proteins

Hoechst staining was employed to assess morphological changes in the nuclei of cells (Fig. 1D). Notable apoptotic features, including diminished cell counts, nuclear condensation, fragmentation, and the appearance of crescent-shaped nuclei, were observed in cells treated with Her. Subsequently, the impact of Her on apoptosis in MCF-7, AGS, and A549 cells was explored. Annexin-PI staining, following Her treatment, showed a significant decrease in viable MCF-7 cells and a marked increase in apoptotic cells, with the most pronounced effects observed at concentrations of 15 and 20 μmol·L^{-1}. In AGS cells, Her treatment led to a proapoptotic effect, evidenced by an increase in the Sub-G_1 cell population and a concurrent decrease in G_1 phase cells, as indicated by the Sub-G_1 DNA content analysis. However, in A549 cells, Her at the same concentrations did not induce notable changes in apoptotic cells or the Sub-G1 cell population. In A549 cells, Her treatment up to 20 μmol·L^{-1} for 24 h inhibited cell proliferation without inducing apoptosis, whereas at 48 h, Her was capable of triggering significant apoptosis (Figs. 1B and 2A). These findings demonstrate that Her effectively inhibits cell growth and exhibits potent cytotoxicity in MCF-7, AGS, and A549 cells.

To elucidate the mechanisms behind the apoptotic cell death induced by Her, we conducted western blot analyses of apoptosis-related proteins. Her treatment led to enhanced apoptosis, evidenced by an elevation in cleaved caspase-3 levels

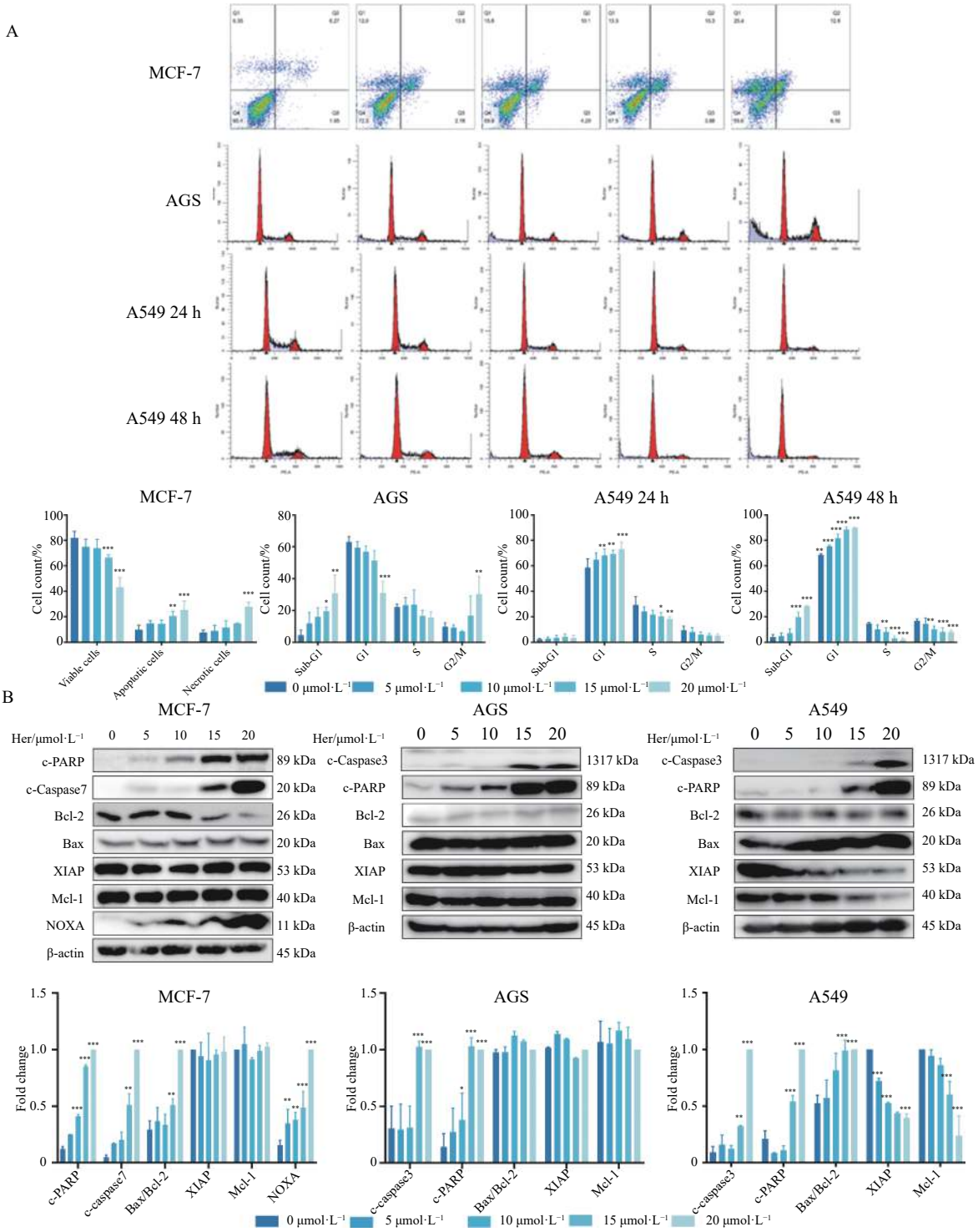

Fig. 2 Effects of Her treatment on apoptosis, cell cycle progression, and apoptosis-related proteins in various cancer cells. (A) Annexin V/PI double staining of MCF-7 cells treated with Her for 24 h, with detection by flow cytometry. AGS cells and A549 were treated with Her for 24 h, and Sub-G1 cells and the cell cycle distribution were detected by PI staining and flow cytometry. (B) MCF-7, AGS, and A549 cells were treated with Her for 24 h, and cell death-related protein expression levels were detected by Western blotting assay. Data are presented as means ± SD （*n* = 3）. $^{*}P < 0.05$, $^{**}P < 0.01$, and $^{***}P < 0.001$ *vs* control.

in AGS and A549 cells and cleaved caspase-7 levels in MCF-7 cells. Furthermore, an increased Bax/Bcl-2 ratio was observed in MCF-7 and A549 cells, along with a rise in caspase-dependent poly (ADP-ribose) polymerase (PARP) cleavage across all three cell lines, indicating the initiation of caspase-mediated apoptosis by Her. These observations were corroborated by an upregulation of NOXA expression in MCF-7 cells. Additionally, a downregulation of the anti-apoptotic

proteins XIAP and Mcl-1 was noted in A549 cells. Collectively, these results demonstrate that Her triggers apoptosis through the activation of mitochondrial-regulated apoptosis pathways (Fig. 2B).

Her induced ROS production and activated the AMPK and mitogen-activated protein kinase (MAPK) pathways

AMPK plays a crucial role in triggering autophagy in response to various forms of cellular stress. According to our western blot analysis, AMPK phosphorylation levels significantly increased, peaking at 3 h or 6 h following Her administration across all tested cell lines (Fig. 3A). Recent research has illuminated that AMPK can modulate MAPK signaling pathways in cancer cells by phosphorylating key components such as JNK, ERK, and p38. This modulation influences not only the development of cancer but also the efficacy of cancer treatments [18]. Early-stage treatment with Her resulted in elevated expression levels of p-JNK, p-ERK, and p-p38 in MCF-7 cells. The phosphorylation levels of JNK, ERK, and p38 escalated with increasing Her concentrations (Fig. 3A). Similarly, expressions of p-JNK and p-p38 were heightened in AGS and A549 cells, whereas p-ERK levels increased in AGS cells but decreased in A549 cells (Fig. 3A). Furthermore, DCFH-DA staining, which serves as an indicator of oxidative stress, demonstrated that Her treatment enhanced reactive oxygen species (ROS) generation in a dose-dependent manner, reaching a zenith at 3 h in MCF-7 cells (Fig. 3B). This increased oxidative stress was associated with a significant loss in MMP, suggesting defective mitochondrial membrane integrity that would lead to the selective degradation of mitochondria (Fig. 3B). This escalation in oxidative stress correlated with a marked reduction in MMP, indicating compromised mitochondrial membrane integrity that could lead to selective mitochondrial degradation (Fig. 3B). Hence, Her's stimulatory effects lead to ROS production, mitochondrial impairment, and activation of the MAPK signaling pathway. Additionally, Her promoted the formation of autophagosomes through the AMPK pathway during the initial stage of autophagy.

Her triggered autophagy and mitophagy

We further explored the influence of Her on autophagy, a process intimately linked to cell death and energy metabolism. Our findings indicated that escalating concentrations of Her elevated the expression of MAP1LC3/LC3B-II across all three cell lines examined (Fig. 4A). The formation of the ATG12-ATG5-ATG16L complex signifies the early stage of autophagosome formation. In MCF-7 cells, Her was observed to dose-dependently increase ATG12-ATG5 expression starting from 1 h (Fig. 4B). As indicated in Fig. 3B, there was an increase in mitochondrial membrane permeability. The autophagy machinery identifies damaged or dysfunctional mitochondria for removal *via* mitophagy; this process involves the accumulation of PINK1 on depolarized mitochondria, leading to the phosphorylation of ubiquitin, which in turn activates Parkin, triggering the mitophagy pathway to eliminate compromised mitochondria [19]. To examine various proteins involved in mitophagy, we examined various indicators of mitophagy (Fig. 5A). Significant increases in BNIP3L/Nix, BNIP3, PINK1, Parkin, and NDP52 were observed with escalating concentrations of Her (0–20 μmol·L^{-1}). Phospho-ubiquitin levels were notably higher in Her-treated MCF-7 cells compared to control cells (Fig. 5A). Additionally, Optineurin expression was not elevated in cells treated with Her, suggesting a more pivotal role for NDP52, BNIP3, and Nix in the selective recognition of autophagic cargo. To verify Her's role in promoting excessive mitophagy in cancer cells, we assessed the mitochondrial association with the LC3 protein (Fig. 5B). Post-Her treatment, the colocalization of MitoTracker and LC3 was observed. Notably, yellow puncta indicative of this colocalization were also seen with the combined treatment of Her and HCQ, an innovative lysosomal autophagy inhibitor, as well as with Her treatment alone. The use of Rapa, an agent that enhances autophagosome formation, in conjunction with Her, significantly intensified the colocalization of MitoTracker and LC3. This colocalization was similarly observed in AGS and A549 cells (Fig. 5C). Collectively, these results underscore the activation of autophagy by Her, including mitophagy, as evidenced by increased LC3 lipidation and mitophagy markers.

Her induced autophagic flux blockade by lysosome dysfunction

In our examination of Her's impact on autophagic flux, we observed a significant elevation in SQSTM1/p62 expression, indicating an inhibitory effect on the late stage of autophagy (Fig. 4A). The concurrent increase in both LC3-II and p62 levels suggests an impediment to autophagic flux, as normally, p62 would be degraded during the later stage of autophagy. Consequently, we also assessed the expression of lysosomal membrane markers in cells treated with Her. We discovered that LAMP1 expression increased in MCF-7 and A549 cells or remained stable in AGS cells, implying that the autophagy-lysosomal membrane integrity was preserved and lysosomal formation was potentially enhanced. Nonetheless, the maturation of Cathepsin D (CTSD), a measure of lysosomal functionality, was disrupted, with an increase in pro-CTSD expression following Her treatment, indicative of impaired lysosomal degradation capabilities (Fig. 4A).

Given the accumulation of p62, we employed an RFP-GFP-LC3 reporter assay to scrutinize autophagic flux in cells exposed to Her. This assay reveals autophagosome formation through the visibility of both RFP and GFP signals, presenting as yellow puncta. Upon the fusion of autophagosomes with lysosomes, the acidic environment quenches GFP signals, leaving only RFP signals and thus red autolysosomes visible. Our findings indicated that Her treatment prompted an increase in RFP-only puncta (red), denoting autolysosome fusion, and heightened autophagosome formation (yellow). The prevalence of yellow puncta suggests that Her treatment obstructs the late stage of autophagy, specifically by hindering the degradation process within autolysosomes (Fig. 6A).

To elucidate the mechanism underlying the blockade of autophagic flux, we assessed the fusion of autophagosomes

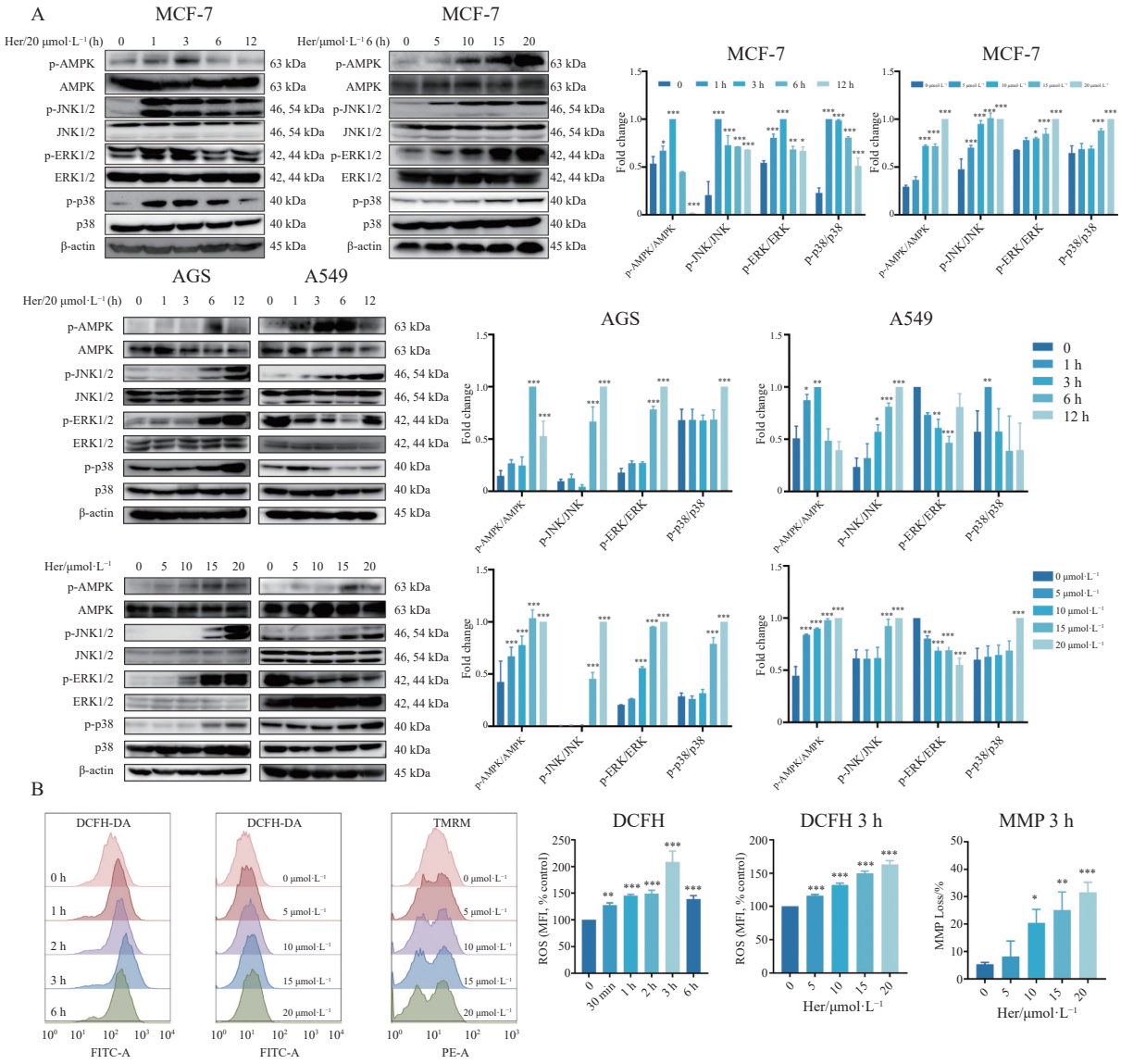

Fig. 3 Her induced ROS production and the expression of proteins related to the AMPK and MAPK pathways. (A) AMPK and MAPK signaling pathway expression for Her dose- and time-course experiments and statistical analysis of Western blotting results. (B) ROS generation was evaluated by DCFH, and MMP loss was detected by TMRM. MCF-7 cells were treated with Her at various doses and for various durations. Data are presented as means ± SD (n = 3) . $^{*}P < 0.05$, $^{**}P < 0.01$, and $^{***}P < 0.001$ *vs* control.

and lysosomes through LC3-LysoTracker and LC3-LAMP1 colocalization in Her-treated MCF-7 cells. Notably, the colocalization between LysoTracker and LC3 markedly increased in cells treated with Her, signifying that the fusion of autophagosomes and lysosomes was not impeded by Her treatment. This indicates that the mechanism by which Her disrupts autophagic flux does not involve the inhibition of autophagosome and lysosome fusion (Fig. 6B). Similarly, LAMP1, a lysosomal membrane marker, exhibited significantly enhanced colocalization with LC3 in MCF-7 cells following Her treatment (Fig. 6C). This further confirms that lysosomal fusion with mitophagosomes remains unaffected by Her, as evidenced by the colocalization of LAMP1 and MitoTracker (Fig. 6D). The maturation of cathepsins typically relies on an acidic lysosomal environment, making an increase in lysosomal pH a critical sign of lysosomal dysfunction. To detect changes in lysosomal pH, we utilized LysoSensor DND-160 (Fig. 6E) and acridine orange (AO) staining (Fig. 6F). Diminished LysoSensor yellow fluorescence and decreased red AO staining demonstrated that Her compromised the acidic conditions within lysosomes.

These findings suggest that Her impedes the degradation of autophagic cargo in these cancer cells by compromising lysosomal functional capacity, thereby obstructing autophagic flux.

Programmed cell death caused by Her and the role of noncanonical autophagy

To explore whether mitochondrial damage induced by

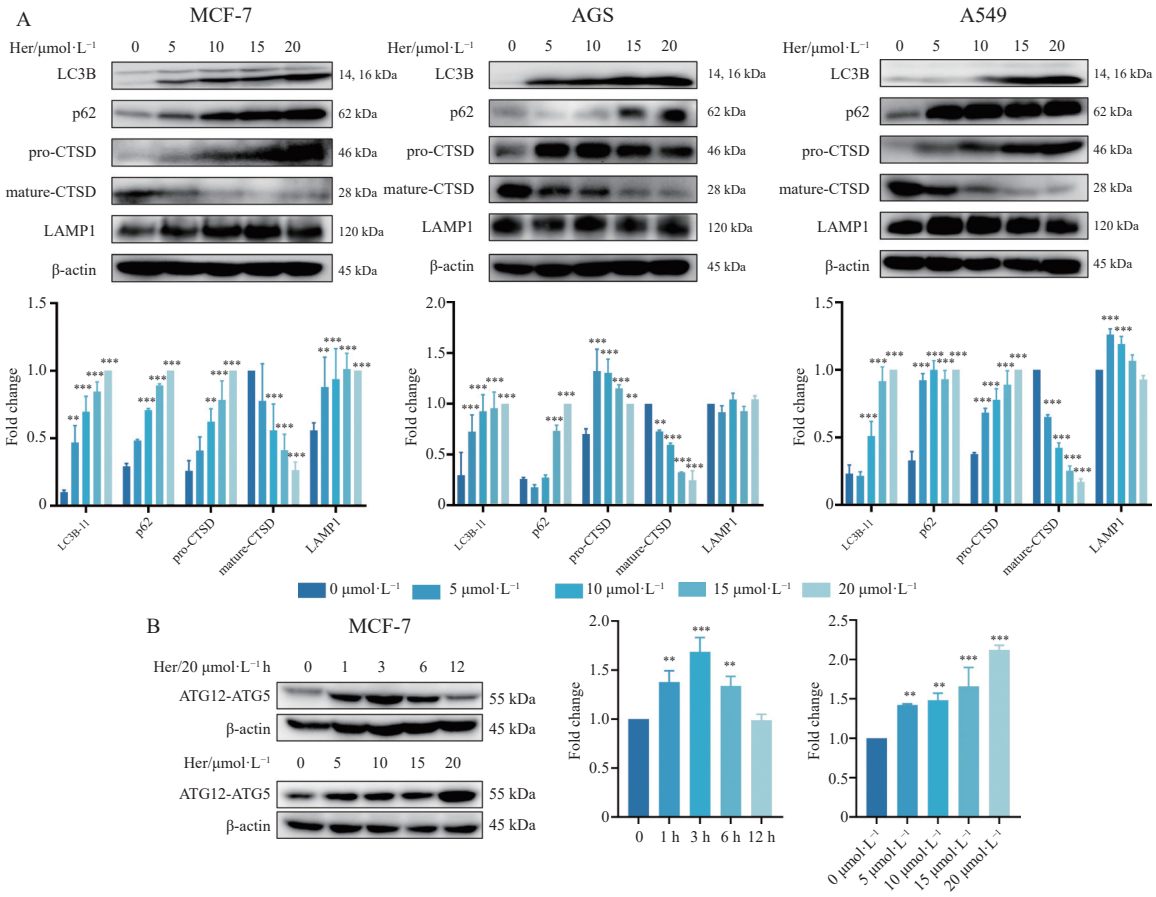

Fig. 4 Her induced autophagy and changed the expression of autophagy and lysosome-related proteins. (A) MCF-7 cells were treated with Her for 24 h, and autophagy and lysosome marker proteins were detected by western blotting. (B) ATG12-ATG5 was evaluated by western blotting. In each bar graph, data are presented as means ± SD ($n = 3$). $^{*}P < 0.05$, $^{**}P < 0.01$, and $^{***}P < 0.001$ *vs* control.

Her influences apoptotic cell death, we pre-treated cells with specific inhibitors of cell death prior to Her exposure. Z-VAD-FMK, a pan-caspase inhibitor, along with Nec-1 and NSA, inhibitors of necroptosis, effectively mitigated Her-induced cell death in MCF-7 cells, enhancing cell viability (Fig. 7A). Z-VAD-FMK also prevented the activation of cleaved-caspase 7 and cleaved-PARP, indicating its role in blocking apoptosis. However, the levels of LC3II and p62 remained elevated (Fig. 7C). These observations imply that Her triggers both apoptosis and necroptosis, suggesting that apoptosis does not precede autophagy or is not directly linked to it. Additionally, the ROS scavenger NAC was able to suppress Her-induced apoptosis (Figs. 7A ,C), further indicating the role of oxidative stress in the apoptotic process initiated by Her.

We also applied an early step inhibitor of canonical autophagy, 3-MA, and observed no effect on cell death, LC3 lipidation, or p62, suggesting that noncanonical autophagy may be involved. Therefore, we examined an early autophagy event, ATG5-ATG12 binding to ATG16L1, which is necessary for autophagosome formation and LC3 lipidation in both the canonical and noncanonical pathways. ATG16L1 puncta were observed in Her-treated cells and cells treated with both Her and 3-MA but not in Baf A1-treated cells (Fig. 7B). Baf A1 is a lysosome inhibitor, a V-ATPase inhibitor, and blocks noncanonical autophagy and LC3 lipidation [20, 21]. As expected, Her-induced LC3 lipidation was abolished by Baf A1 treatment. Compound C (CC), an AMPK inhibitor, was also used to suppress autophagosome formation. The results showed that the LC3 lipidation caused by Her was inhibited by treatment with CC, whereas cell death and expression of cleaved-caspase7 and cleaved-PARP were enhanced (Fig. 7C). Additionally, pre-incubation with HCQ did not rescue cells from death and affected the expression of LC3 and p62 (Fig. 7A). These results indicated a similar role of Her and HCQ in blocking the autophagic flux. Both apoptosis and necroptosis may contribute to Her-induced cell death, and the potential role of noncanonical autophagy should be considered.

Discussion

Extensive research has focused on the biological effects of natural products sourced from plants and other origins [22]. In the context of cancer therapy, natural medicinal compounds are favored for their ability to selectively target cancer cells through various mechanisms and to enhance immune responses, all while presenting fewer side effects com-

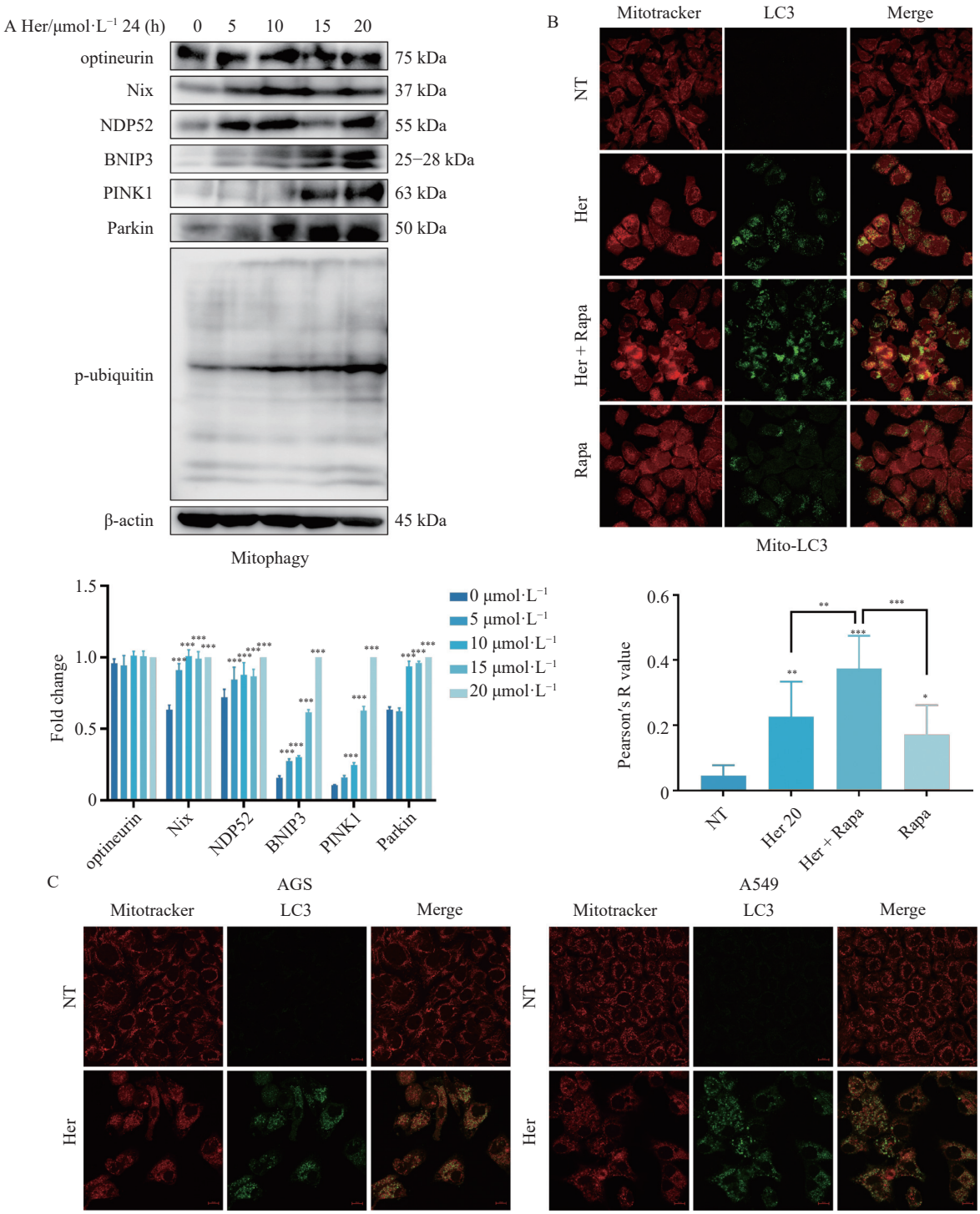

Fig. 5 Effects of Her treatment on mitophagy-related protein markers. (A) Mitophagy marker proteins were detected by Western blotting assay in MCF-7 cells treated with Her for 24 h. Mitophagy was evaluated based on the colocalization of MitoTracker (red) and LC3 (green) by confocal microscopy (630 ×) in (B) MCF-7 cells and (C) AGS and A549 cells. Three independent experiments were performed and representative results from one experiment are shown. In each bar graph, data are presented as means ± SD ($n = 3$). $^{*}P < 0.05$, $^{**}P < 0.01$, and $^{***}P < 0.001$ *vs* control.

pared to traditional treatment methods [23]. The potential anticancer properties of Her have only recently come to light, with a limited number of studies examining the autophagy induced by Her in cancer contexts. The intricate processes by which Her facilitates cell death and the specific involvement of autophagy remain largely unexplored. Our study marks the first to illustrate that Her initiates the activation of noncanonical autophagy yet impedes autophagic flux at a later stage by inhibiting autolysosome functionality, thereby inducing cancer cell death. We demonstrated that Her triggers mitochon-

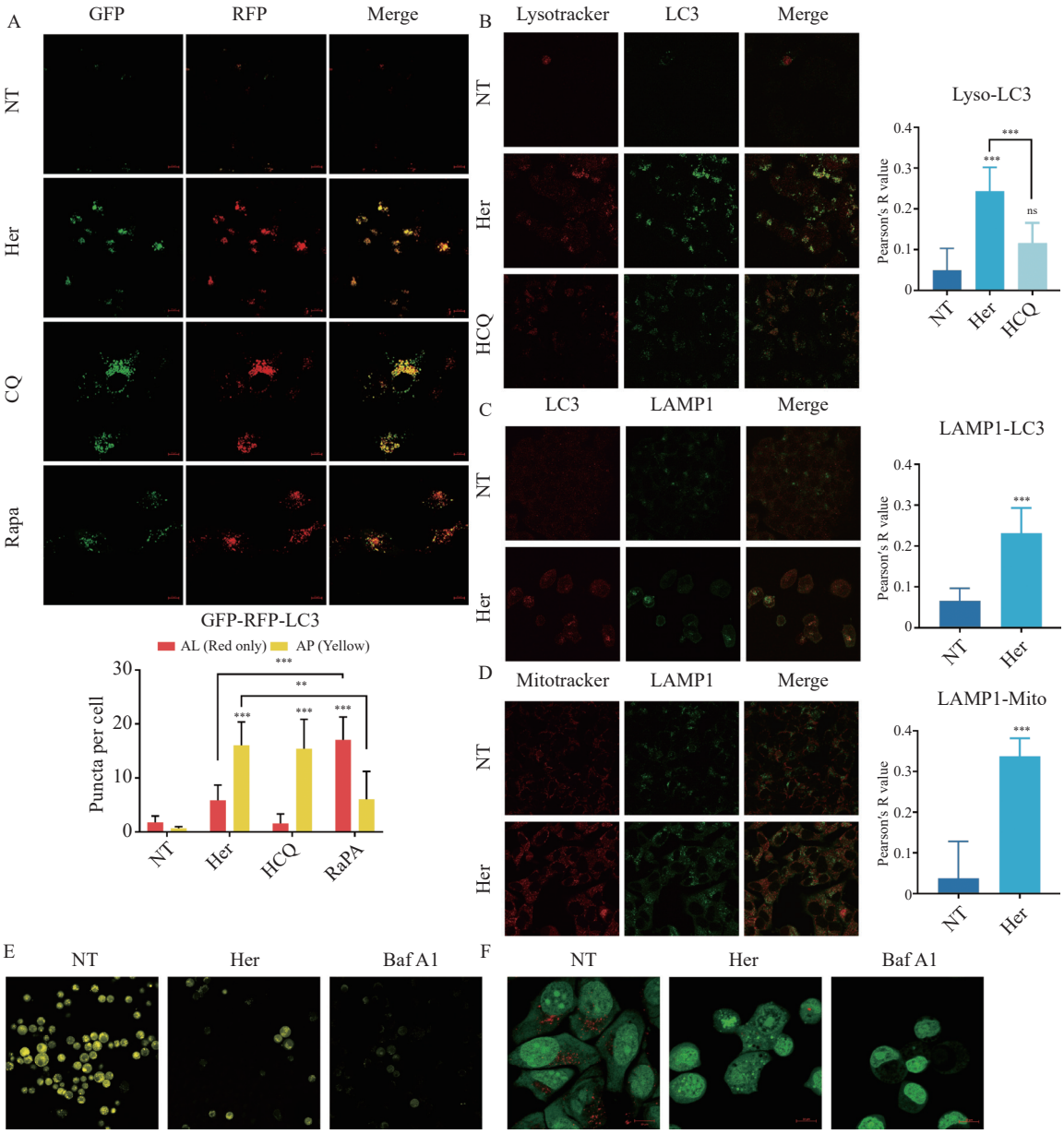

Fig. 6 Her impaired autophagic flux by blocking autolysosome degradation. (A) Autophagic flux was detected by RFP-GFP-LC3 and confocal microscopy (630 ×). MCF-7 cells were treated with Her or HCQ for 24 h. RFP-GFP-LC3-labeled autophagosomes (AP) are shown in yellow. GFP was quenched under an acidic environment; accordingly, red puncta were autolysosomes (AL). Evaluated from at least three different areas. (B) Colocalization of LC3 (green) and Lysotracker Red was examined by confocal microscopy (630 ×) in MCF-7 cells treated with Her or HCQ for 24 h. (C) Colocalization of LC3 (red) and LAMP1 (green) was examined by confocal microscopy (630 ×) in MCF-7 cells treated with Her for 24 h. (D) Colocalization of MitoTracker (red) and LAMP1 (green) was checked by confocal microscopy (630 ×) in MCF-7 cells treated with Her for 24 h. (E) Images of LysoSensor DND-160 and yellow fluorescence in low pH environments. (F) Images of AO staining. AO can bind to intracellular low-pH organelles, such as lysosomes, showing red fluorescence. Data are presented as means ± SD (n = 3). $^{*}P < 0.05$, $^{**}P < 0.01$, and $^{***}P < 0.001$ *vs* control.

drial damage, autophagy, and mitophagy. Additionally, our findings reveal that Her instigates both apoptosis and necroptosis, indicating that multiple forms of cell death play a role in Her's cytotoxic effects (Fig. 8).

The specific effects of Her on autophagy, particularly its influence on autophagy flux and noncanonical autophagy pathways, remain poorly understood. Our findings reveal that Her mediates cell death through the initial induction of autophagosome formation and subsequent inhibition of late-stage autophagy due to lysosomal dysfunction, while not hindering autolysosome formation. Autophagy serves as an intracellular system for removing waste, initiated by the formation of autophagosomes through several distinct phases: phagophore initiation, nucleation, elongation, and closure. During phago-

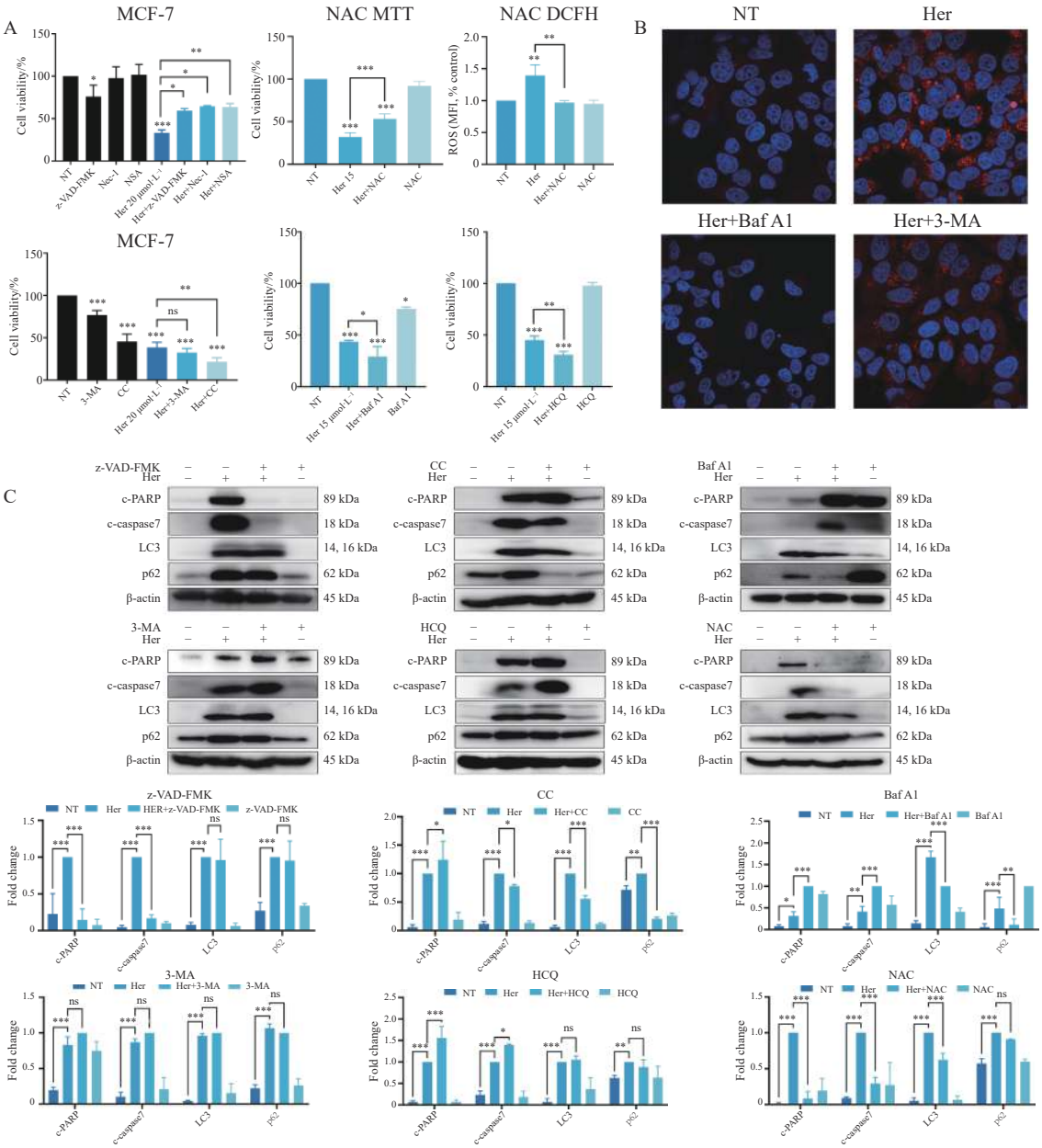

Fig. 7 Effects of specific cell death inhibitors and the involvement of the noncanonical pathway on Her treatment. (A) Cell viability was detected by an MTT assay. Cells were pre-treated with the pan-caspase inhibitor Z-VAD-FMK (50 μmol·L^{-1}), the AMPK inhibitor CC (10 μmol·L^{-1}), the autophagy inhibitors 3-MA (5 mmol·L^{-1}), Baf A1 (100 nmol·L^{-1}), and HCQ (40 μmol·L^{-1}), or the ROS scavenger NAC (10 mmol·L^{-1}) for 1 h and then treated with Her for 24 h. (B) ATG16L1 (red) and nuclei (Hoechst 33258) were checked by confocal microscopy (630 ×) in MCF-7 cells pre-treated with Baf A1 or 3-MA for 1 h and then treated with Her for 24 h. (C) Analyses of apoptosis- and autophagy-related proteins after treatment with inhibitors. In each bar graph, data are presented as means ± SD (n = 3). $^{*}P < 0.05$, $^{**}P < 0.01$, and $^{***}P < 0.001$ *vs* control.

phore initiation, nutrient deprivation-induced AMPK activation leads to the formation of the ULK1 complex. The Beclin 1 complex, comprising Beclin 1, VPS34, VPS15, and ATG14, participates in phagophore nucleation, while phagophore elongation is facilitated by two conjugation systems: ATG5-ATG12:ATG16L1 and ATG8 [24, 25]. Our research, along with findings from others [11, 13], confirms that Her robustly induces and activates AMPK, thereby stimulating several downstream pathways related to cell death, including MAPK signaling and mTOR signaling inhibition. This activation likely enhances autophagosome formation and disrupts MMP, prompting the excessive initiation of mitophagy. Our data suggest that AMPK plays a pivotal role in the Her-induced cascade of multi-type cell death, positioning it as a crucial molecular target for eliminating aggressive cancer cells. The ATG5-ATG12-ATG16L1 complex, indicative of phagophore elongation but not mature autophagosome formation [26], highlights that Her promotes pre-autophagosome as-

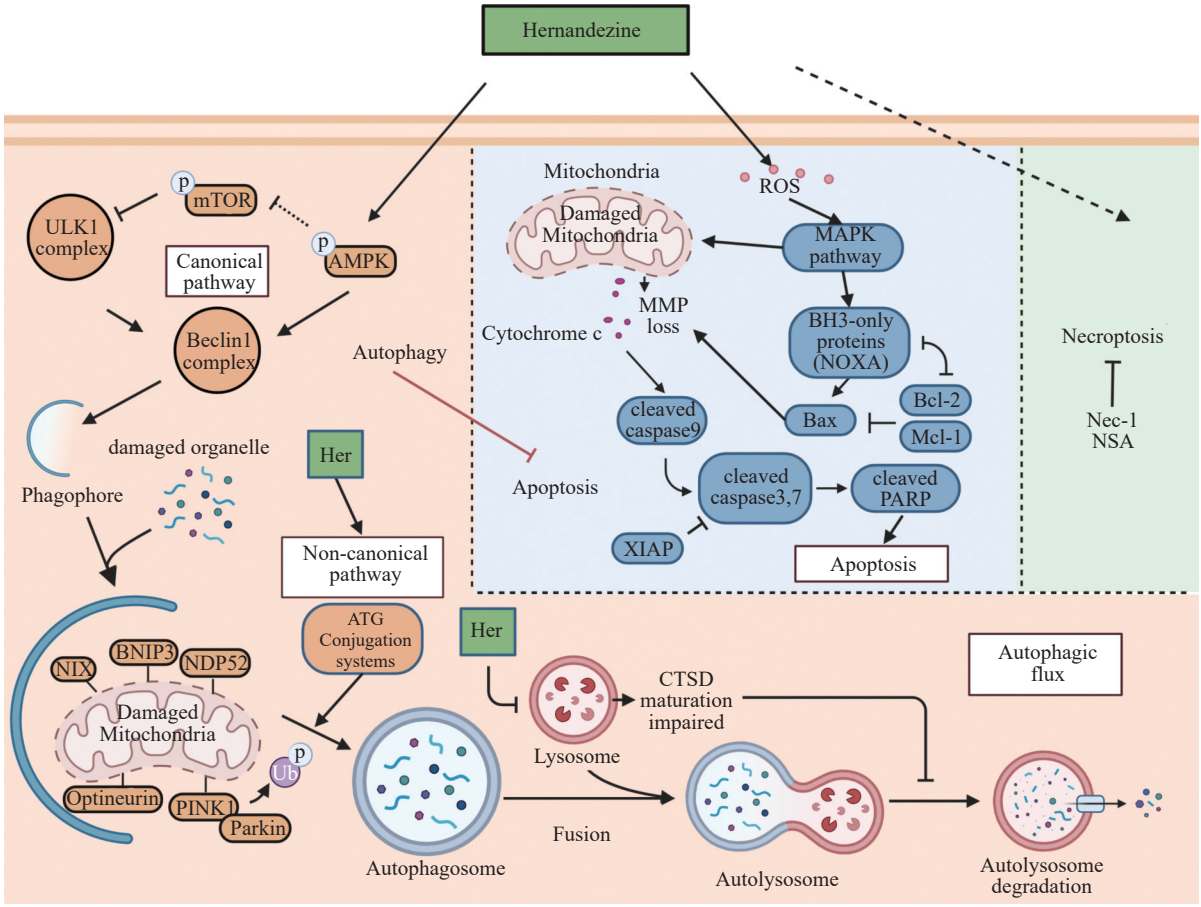

Fig. 8 Line diagram showing the proposed molecular mechanism underlying Her-induced cancer cell death.

sembly at very early stage, as evidenced by increased ATG12-ATG5 expression and ATG16L1 recruitment. However, autophagy in cancer cells is associated with chemoresistance and recurrence [27]. Thus, a therapeutic strategy that disrupts autophagy or sustains autophagy induction could lead to the accumulation of ubiquitinated proteins, dysfunctional mitochondria, and elevated ROS levels, resulting in significant cytotoxic effects. Our findings demonstrated that Her elevated ROS levels and enhanced MMP loss across three cancer cell types, inducing cell death. Moreover, we showed that Her treatment impaired late-stage autophagic processes, suggesting a complex interplay between autophagy regulation and cancer cell viability influenced by Her.

Impaired autophagic flux can occur through two primary mechanisms: (1) inhibition of the fusion between autophagosomes and lysosomes and (2) disruption of autolysosome degradation, which involves interference with lysosomal functionality. For example, berbamine, a bisbenzylisoquinoline alkaloid, impedes the fusion of autophagosomes and lysosomes by inhibiting SNARE complex formation [28]. In our study, both autolysosomes and autophagosomes accumulated following Her treatment. Using RFP-GFP-LC3 assays and assessing the colocalization of LC3 with lysosomes, we determined that the fusion of autophagosomes and lysosomes was not affected by Her treatment; rather, it was the degradation process within autolysosomes that was compromised. Lysosomal acidification is crucial for the degradation activity of autolysosomes, with the maturation of cathepsins dependent on an acidic environment. Her treatment disrupted this acidic milieu, thereby hindering the degradation process in autolysosomes. Lysosomal hydrolases, such as cathepsins, play an essential role in the breakdown of autolysosomal contents, thereby facilitating autophagic flux [29]. After treatment with Her, there was an upregulation of pro-CTSD and a concurrent decrease in mature-CTSD. Thus, Her impedes the degradation of autolysosomes by compromising lysosomal function, specifically through the disruption of lysosomal acidification and inhibition of CTSD maturation.

Incomplete autophagy can lead to the accumulation of damaged organelles, particularly mitochondria, which might result in mitochondria-mediated cell death or mitophagy. Mitochondria play a vital role in the rapid proliferation and high metabolic demands of cancer cells, and their dysfunction can trigger cell death. Mitophagy, a specialized autophagic process, ensures the selective elimination of impaired mitochondria, maintaining cellular health [19]. Our study has revealed that Her treatment significantly upregulates several proteins critical for mitophagy. BNIP3L/Nix and BNIP3, mitochondrial proteins, are pivotal in the initiation of mitophagy [30]. Notably, the levels of Nix and BNIP3 were elevated in Her-

treated MCF-7 cells compared to controls. PINK1, a mitochondrial serine/threonine kinase, stabilizes on the outer membrane of damaged mitochondria, making it a key target in cancer therapy [31]. PINK1 phosphorylates substrates such as the E3 ubiquitin ligase Parkin and ubiquitin itself. These ubiquitinated proteins are then recognized by cargo receptors like optineurin and NDP52 [31]. A decrease in MMP facilitates the accumulation of PINK1 and the recruitment of Parkin to damaged mitochondria. Parkin, in turn, recruits the autophagic adaptor protein SQSTM1/p62, which links to both ubiquitin and LC3, clustering the damaged mitochondria for their subsequent clearance through mitophagy. Our findings demonstrate that Her not only upregulates PINK1 and Parkin but also leads to the accumulation of phospho-ubiquitin and the colocalization of LC3 with the mitochondrial membrane. These results indicate that Her triggers mitophagy in these cancer cells, underscoring its potential efficacy as an anticancer agent.

Recent studies have highlighted numerous compounds that stimulate autophagosome formation while concurrently hindering autophagic flux [32–35]. Her possesses a unique chemical structure distinct from these compounds, and, to the best of our knowledge, analogous effects have not been previously reported for other bisbenzylisoquinoline alkaloids. Autophagy Modulator with Dual Effect-1 (AMDE-1) operates through both canonical and noncanonical autophagy pathways to induce autophagosome generation; however, it also blocks the degradation process by inhibiting lysosomal cathepsin B [20, 35]. Our findings reveal that Her can upregulate phosphorylated AMPK (p-AMPK) and increase ATG16L1 puncta while inhibiting lysosomal acidification and the maturation of CTSD. Intriguingly, akin to AMDE-1's mechanism, the canonical autophagy inhibitor 3-MA had no impact on Her-induced LC3 lipidation and only partially reduced the formation of ATG16L1 puncta, suggesting that Her might also promote noncanonical autophagy pathways. Furthermore, Bafilomycin A1 (Baf A1), a V-ATPase inhibitor and a blocker of noncanonical autophagy, significantly mitigated the Her-induced alterations in ATG16L1 and LC3 lipidation, thereby intensifying cell death. Additionally, CC, an AMPK inhibitor, curtailed the LC3 lipidation triggered by Her and enhanced cleaved-PARP levels. These observations indicate that Her initiates autophagy through both canonical and noncanonical pathways, which appear to have a cytoprotective function. Nevertheless, the mechanisms underlying noncanonical autophagy remain largely elusive.

Our findings highlight that Her induces caspase-dependent apoptosis, as evidenced by the effectiveness of the pan-caspase inhibitor Z-VAD-FMK, alongside necroptosis in cancer cells. This dual induction contrasts with the caspase-independent cell death mechanisms reported in previous studies. Given the capacity of cancer cells to develop resistance to chemotherapy [26], thereby evading cell death, compounds like Her, which can initiate multiple forms of cell death, are potentially more effective against cancer than those targeting a single death pathway. Necroptosis, a form of regulated necrosis mediated by receptor-interacting protein (RIP) kinases, serves as an alternative cell death pathway. It often comes into play when apoptosis is inhibited, either naturally or due to the development of resistance to proapoptotic chemotherapy agents [36]. Our research indicates that Her not only increases the levels of several proapoptotic proteins but also that the use of inhibitors for both apoptosis and necroptosis can partially mitigate cell death.

Our findings present a nuanced perspective on Her's effects, contrasting with reports that Her predominantly induces autophagic death in most cell lines, alongside promoting autophagic flux [10–12]. The accumulation of LC3II, often associated with the onset of autophagy, can also result from inhibited degradation processes. Hence, its detection should be complemented with assessments of autophagic flux, such as p62 expression analysis, GFP-RFP-LC3 assays, the use of autophagy inhibitors, and evaluations of lysosomal functionality. A recent investigation revealed that in pancreatic cancer cells, Her initiates autophagic cell death by activating the ROS/AMPK signaling pathway, which is characterized by decreased p62 levels and increased LC3II accumulation. Notably, the accumulation of LC3II was further enhanced by late-stage autophagy inhibitors like HCQ and Baf A1 [11]. In a separate study, Her was found to inhibit melanoma cell proliferation and induce apoptosis via the JAK2/STAT3 pathway, leading to cell cycle arrest in the G0/G1 phase [12]. Elevated LC3II expression and detection of autophagosome generation via electron microscopy confirmed that Her triggered autophagy, and both the autophagy inhibitor 3-MA and the AMPK inhibitor CC inhibited Her-induced apoptosis, demonstrating that Her activates autophagic cell death in melanoma cells. The results of the above studies differed from ours in terms of autophagic flux in MCF-7, AGS, and A549 cells, and the inhibitors did not behave in the same way, which may have been due to the different roles of Her in different cell lines.

Autophagy is a dynamic and complex process with many influencing factors. To fully elucidate the effects of Her on autophagy, a more complete and thorough method of detection is needed, and in future studies, electron microscopy observation and genetic knockdown or knockout of autophagic genes need to be performed in order to study autophagy more directly and in-depth. Further investigation of the effects of Her on normal cells, in necroptosis, and as part of *in vivo* studies will be required.

Conclusion

In conclusion, Her has been demonstrated to initiate apoptosis and necroptosis in cancer cells, primarily through ROS production and mitochondrial impairment. It also triggers the onset of autophagy and mitophagy, engaging both canonical and noncanonical pathways. Furthermore, Her disrupts autophagic flux by compromising the lysosomal acidic environment and hindering the maturation of CTSD, leading to the buildup of dysfunctional autolysosomes. These insights, presented for the first time, reveal that Her obstructs autophagic flux by impairing lysosomal function, thereby promoting cancer cell death. This study offers novel perspect-

ives on the interplay between apoptosis and autophagy and its potential implications for enhancing cancer treatment strategies.

References

[1] Sung H, Ferlay J, Siegel RL, *et al*. Global cancer statistics 2020: globocan estimates of incidence and mortality worldwide for 36 cancers in 185 countries [J]. *CA Cancer J Clin*, 2021, **71**(3): 209-249.

[2] Housman G, Byler S, Heerboth S, *et al*. Drug resistance in cancer: an overview [J]. *Cancers*, 2014, **6**(3): 1769-1792.

[3] Li M, Wu C, Muhammad JS, *et al*. Melatonin sensitises shikonin-induced cancer cell death mediated by oxidative stress via inhibition of the SIRT3/SOD2-AKT pathway [J]. *Redox Biol*, 2020, **2020**(36): 101632.

[4] Zakki SA, Muhammad JS, Li JL, *et al*. Melatonin triggers the anticancer potential of phenylarsine oxide *via* induction of apoptosis through ROS generation and JNK activation [J]. *Metallomics*, 2020, **12**(3): 396-407.

[5] Fuchs Y, Steller H. Live to die another way: modes of programmed cell death and the signals emanating from dying cells [J]. *Nat Rev Mol Cell Biol*, 2015, **16**(6): 329-344.

[6] Wong SQ, Kumar A V, Mills J, *et al*. Autophagy in aging and longevity [J]. *Hum Genet*, 2020, **139**(3): 277-290.

[7] Chi KH, Wang YS, Huang YC, *et al*. Simultaneous activation and inhibition of autophagy sensitizes cancer cells to chemotherapy [J]. *Oncotarget*, 2016, **7**(36): 58075-58088.

[8] Lemasters JJ. Selective mitochondrial autophagy, or mitophagy, as a targeted defense against oxidative stress, mitochondrial dysfunction, and aging [J]. *Rejuvenation Res*, 2005, **8**(1): 3-5.

[9] Fodale V, Pierobon M, Liotta L, *et al*. Mechanism of cell adaptation [J]. *Cancer J*, 2011, **17**(2): 89-95.

[10] Kuok C, Wang Q, Fong P, *et al*. Inhibitory effect of Hernandezine on the proliferation of hepatocellular carcinoma [J]. *Biol Pharm Bull*, 2023, **46**(2): 245-256.

[11] Song C, Hu Y, Mang Z, *et al*. Hernandezine induces autophagic cell death in human pancreatic cancer cells via activation of the ROS/AMPK signaling pathway [J]. *Acta Pharmacol Sin*, 2023, **44**(4): 865-876.

[12] Wang X, Li X, Xia Y, *et al*. Hernandezine regulates proliferation and autophagy-induced apoptosis in melanoma cells [J]. *J Nat Prod*, 2022, **85**(5): 1351-1362.

[13] Law BYK, Mok SWF, Chan WK, *et al*. Hernandezine, a novel AMPK activator induces autophagic cell death in drug-resistant cancers [J]. *Oncotarget*, 2016, **7**(7): 8090-8104.

[14] Law BYK, Michelangeli F, Qu YQ, *et al*. Neferine induces autophagy-dependent cell death in apoptosis-resistant cancers *via* ryanodine receptor and Ca^{2+}-dependent mechanism [J]. *Sci Rep*, 2019, **9**(1): 20034.

[15] Wu JM, Chen Y, Chen JC, *et al*. Tetrandrine induces apoptosis and growth suppression of colon cancer cells in mice [J]. *Cancer Lett*, 2010, **287**(2): 187-195.

[16] Zhao Y, Lv JJ, Chen J, *et al*. Berbamine inhibited the growth of prostate cancer cells *in vivo* and *in vitro via* triggering intrinsic pathway of apoptosis [J]. *Prostate Cancer Prostatic Dis*, 2016, **19**(4): 358-366.

[17] Riccardi C, Nicoletti I. Analysis of apoptosis by propidium iodide staining and flow cytometry [J]. *Nat Protoc*, 2006, **1**(3): 1458-1461.

[18] Yuan J, Dong X, Yap J, *et al*. The MAPK and AMPK signalings: interplay and implication in targeted cancer therapy [J]. *J Hematol Oncol*, 2020, **13**(1): 113.

[19] Vara-Perez M, Felipe-Abrio B, Agostinis P. Mitophagy in cancer: a tale of adaptation [J]. *Cells*, 2019, **8**(5): 493.

[20] Gao Y, Liu Y, Hong L, *et al*. Golgi-associated LC3 lipidation requires V-ATPase in noncanonical autophagy [J]. *Cell Death Dis*, 2016, **7**(8): e2330.

[21] Jacquin E, Leclerc-Mercier S, Judon C, *et al*. Pharmacological modulators of autophagy activate a parallel noncanonical pathway driving unconventional LC3 lipidation [J]. *Autophagy*, 2017, **13**(5): 854-867.

[22] Safarzadeh E, Sandoghchian SS, Baradaran B. Herbal medicine as inducers of apoptosis in cancer treatment [J]. *Adv Pharm Bull*, 2014, **4**(Suppl 1): 421-427.

[23] Tavakoli J, Miar S, Majid ZM, *et al*. Evaluation of effectiveness of herbal medication in cancer care: a review study [J]. *Iran J Cancer Prev*, 2012, **5**(3): 144-156.

[24] Galluzzi L, Green DR. Autophagy-independent functions of the autophagy machinery [J]. *Cell*, 2019, **177**(7): 1682-1699.

[25] Galluzzi L, Bravo-San Pedro JM, Levine B, *et al*. Pharmacological modulation of autophagy: therapeutic potential and persisting obstacles [J]. *Nat Rev Drug Discov*, 2017, **16**(7): 487-511.

[26] Fujita N, Itoh T, Omori H, *et al*. The Atg16L complex specifies the site of LC3 lipidation for membrane biogenesis in autophagy [J]. *Mol Biol Cell*, 2008, **19**(5): 2092-2100.

[27] Li YJ, Lei YH, Yao N, *et al*. Autophagy and multidrug resistance in cancer [J]. *Chin J Cancer*, 2017, **36**(1): 52.

[28] Fu R, Deng Q, Zhang H, *et al*. A novel autophagy inhibitor berbamine blocks SNARE-mediated autophagosome-lysosome fusion through upregulation of BNIP3 [J]. *Cell Death Dis*, 2018, **9**(2): 243.

[29] Porter K, Nallathambi J, Lin Y, Liton PB (2013) Lysosomal basification and decreased autophagic flux in oxidatively stressed trabecular meshwork cells. Autophagy 9: 581–594. https://doi.org/10.4161/auto.23568.

[30] Mancias JD, Kimmelman AC. Mechanisms of selective autophagy in normal physiology and cancer [J]. *J Mol Biol*, 2016, **428**: 1659-1680.

[31] Lazarou M, Sliter DA, Kane LA, *et al*. The ubiquitin kinase PINK1 recruits autophagy receptors to induce mitophagy [J]. *Nature*, 2015, **524**: 309-314.

[32] Kucharewicz K, Dudkowska M, Zawadzka A, *et al*. Simultaneous induction and blockade of autophagy by a single agent [J]. *Cell Death Dis*, 2018, **9**: 353.

[33] Feng X, Zhou J, Li J, *et al*. Tubeimoside I induces accumulation of impaired autophagolysosome against cervical cancer cells by both initiating autophagy and inhibiting lysosomal function [J]. *Cell Death Dis*, 2018, **9**: 1117.

[34] Ranieri R, Ciaglia E, Amodio G, *et al*. N6-isopentenyladenosine dual targeting of AMPK and Rab7 prenylation inhibits melanoma growth through the impairment of autophagic flux [J]. *Cell Death Differ*, 2018, **25**: 353-367.

[35] Li M, Yang Z, Vollmer LL, *et al*. AMDE-1 Is a dual function chemical for autophagy activation and inhibition [J]. *PLOS ONE*, 2015, **10**: e0122083.

[36] Zhu F, Zhang W, Yang T, *et al*. Complex roles of necroptosis in cancer [J]. *J Zhejiang Univ-Sc B*, 2019, **20**: 399-413.

Cite this article as: FENG Qianwen, SUN Lu, Muhammad Jibran Sualeh, *et al*. Hernandezine promotes cancer cell apoptosis and disrupts the lysosomal acidic environment and cathepsin D maturation [J]. *Chin J Nat Med*, 2024, **22**(5): 387-401.